



ELSEVIER

Physica C 369 (2002) 21–27

PHYSICA C

www.elsevier.com/locate/physc

Vortex dynamics of 2D electron plasmas

C.F. Driscoll*, D.Z. Jin, D.A. Schecter, D.H.E. Dubin

*Department of Physics, Institute of Pure and Applied Physical Sciences, University of California at San Diego,
La Jolla, CA 92093-0319, USA*

Abstract

Electron columns confined magnetically in vacuum evolve in (r, θ) as $N \sim 10^9$ field-aligned rods of charge, or point vortices. Neglecting discreteness, the column evolves as would vorticity in an inviscid, incompressible fluid, governed by the Euler equations. The macroscopic flow dynamics is readily imaged, including effects such as surface waves and inviscid damping, two vortex merger, and gradient-driven vortex motion. Turbulent initial states are observed to relax to “vortex crystal” meta-equilibria, due to vortex “cooling” from entropic mixing of background vorticity; and characteristics of this process are predicted by theory. The microscopic discreteness gives rise to point-vortex diffusion, which is strongly affected by the overall flow shear. Macroscopically and microscopically, the vortex dynamics depends critically on whether the vortex is prograde or retrograde with respect to the flow shear. © 2001 Elsevier Science B.V. All rights reserved.

Keywords: Vortex dynamics; Electron plasma; Euler flow

1. Electron plasmas as Euler flows

Magnetically confined pure electron columns are excellent systems for quantitative observations of 2D fluid vortices, turbulence and self-organization [1]. A “generic” experimental apparatus is shown schematically in Fig. 1. The electrons of density $\tilde{n} \sim 10^7 \text{ cm}^{-3}$ are contained in vacuum ($P \approx 10^{-10}$ Torr) within a grounded conducting wall ($2R_w = 7 \text{ cm}$). A uniform axial magnetic field ($B \lesssim 1 \text{ T}$) provides radial confinement, and negative voltages ($V \approx 50 \text{ V}$) applied to end cylinders provide confinement at the ends. The confined plasma is diagnosed and manipulated by antennas

on the wall. Finally, the z -integrated electron density $n(r, \theta, t)$ is measured (destructively) by accelerating the electrons onto a phosphor screen and imaging the resulting light with a CCD camera.

The (r, θ) flow of the electrons across the magnetic field occurs due to the strong electric field $\mathbf{E}(r, \theta, t) = -\nabla\phi(r, \theta, t)$ from the unneutralized electron plasma. The cross-magnetic-field “drift” velocity is $\mathbf{v}(r, \theta, t) = \mathbf{E} \times \mathbf{B}/B^2$, giving a bulk plasma rotation $f_R(r) \equiv v_\theta(r)/2\pi r \approx 10^4 \text{ s}^{-1}$. Since the individual electrons bounce axially along the magnetic field lines in about $1 \mu\text{s}$, electrons behave as rigid “rods” of charge, or “point vortices” in (r, θ) .

In this approximation, the (r, θ) flow of the electrons is described by the 2D drift-Poisson equations [1], which can be written in terms of the vorticity $\zeta(r, \theta, t) \equiv (4\pi ec/B)n$ and the scaled electrostatic potential $\psi(r, \theta, t) \equiv (c/B)\phi$ as

* Corresponding author.

E-mail address: fdriscoll@ucsd.edu (C.F. Driscoll).

URL: <http://sdphCA.ucsd.edu>.

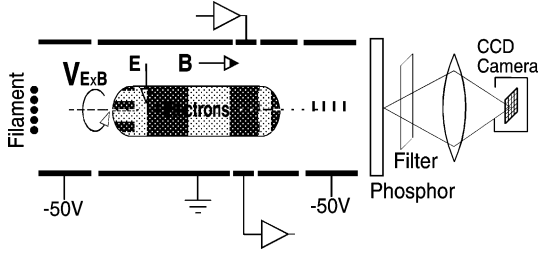


Fig. 1. The cylindrical experimental apparatus with phosphor screen/CCD camera diagnostic.

$$\frac{\partial \zeta}{\partial t} + \mathbf{v} \cdot \nabla \zeta = 0, \quad \mathbf{v} = -\nabla \psi \times \hat{z},$$

$$\nabla^2 \psi = \zeta.$$

These equations are isomorphic to the 2D Euler equations for an incompressible, inviscid fluid. The flow vorticity ζ is proportional to the electron density n , which is directly measured.

A column of electrons in vacuum surrounded by a conducting wall thus evolves as would a 2D vortex in an incompressible inviscid fluid surrounded by a circular *free-slip* boundary. We emphasize that here, there is only one sign of vorticity (taken to be positive), because the density of electrons can only be positive, and there are no charges of opposite sign.

There are also small unwanted drifts due to the end confinement fields [2], and weak “viscous” effects on small spatial scales due to electron–electron collisions [3], but these are *not* modelled by the Euler or the Navier–Stokes equation. This collisional point-vortex diffusion will be described below.

Euler flows are strongly constrained by integral invariants. The total circulation (number of electrons) Γ_{tot} , angular momentum P_θ , and energy H are well conserved in the experiments. However, less robust invariants such as the entropy S and enstrophy Z_2 vary significantly, due to measurement coarse-graining or dissipation of small spatial scales [4].

2. Waves on a vortex

The simplest stable flow is a circular region of vorticity with monotonically decreasing vorticity

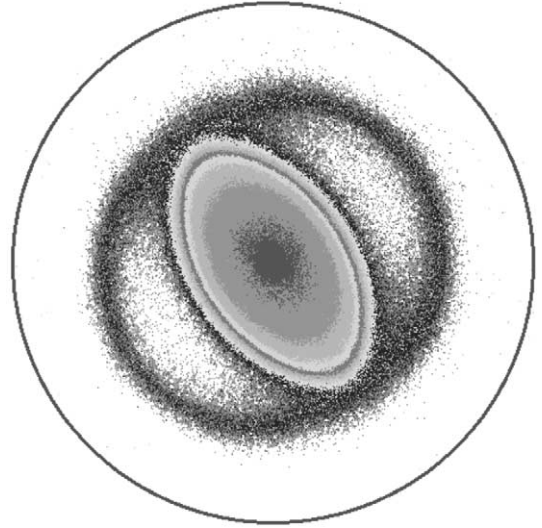


Fig. 2. Measured electron density (vorticity) for an $m = 2$ wave with cat’s eyes from saturated inviscid damping.

profile $\zeta(r)$ and azimuthal flow velocity $\mathbf{v}_\theta(r)$, consisting of 10^9 “point-vortex” electrons. Small shape distortions of this nominally circular vortex can be analyzed as a spectrum of waves with azimuthal and radial mode numbers (m, k) , varying as $g_k(r) \exp(im\theta - i\omega_k t)$.

A large-amplitude $m = 2$ distortion is shown in Fig. 2. These waves are generalizations of the surface distortions on vortex patches referred to as Kelvin waves [5]. Recent analyses have elucidated the process of *inviscid damping* [6,7] due to wave–fluid interactions at critical radii r_c where $\omega_k/2\pi = m f_R(r_c)$, and this damping is routinely observed in electron plasma experiments [8]. These modes have recently been analyzed in terms of “discrete” and “continuum” eigenfunctions [9], with application to atmospheric circulations [10].

For even moderate wave amplitudes, this observed damping is typically non-linear, and the damping may decrease [7,8] or cease when the resulting “cat’s-eye” flows generate fine-scale filaments inside the vortex. For “sharp-edged” vorticity profiles, the resonant radii r_c can be completely outside the vortex, in which case no direct resonance damping occurs except at large amplitudes, as shown in Fig. 2. Also, experiments have shown the importance of non-linear wave–wave cou-

plings: even otherwise stable modes may exhibit “beat-wave damping” [11], whereby energy is observed to flow to longer azimuthal wavelengths.

If the vorticity profile $\zeta(r)$ is “hollow” rather than monotonically decreasing, some of these modes may be unstable, giving the Kelvin–Helmholtz (shear-flow) instability [12,13]. Both the frequencies and growth rates of these unstable modes are reasonably well characterized by computational solution of the eigenvalue equation using the measured density profiles [14]. One exception is $m = 1$, where we observe a robust exponential instability [15] where cold fluid theory predicts only algebraic growth; here, finite length effects may cause the instability [16,17].

3. Vortex merger

The merger of like-sign macroscopic vortices as shown in Fig. 3 is fundamental to the relaxation of 2D turbulence at high Reynolds numbers. Experimentally [4], two vortices are observed to merge within a few orbit times when the spacing between vortex centers D is less than 1.6 times the individual vortex diameter $2R_v$; and to orbit without merger for more than 10^4 orbits when $D/2R_v > 1.7$. Of course, point vortices with $R_v = 0$ could never merge. The merger after 10^4 orbits apparently results from weak non-ideal effects causing R_v to increase, thereby satisfying $D/2R_v < 1.6$.

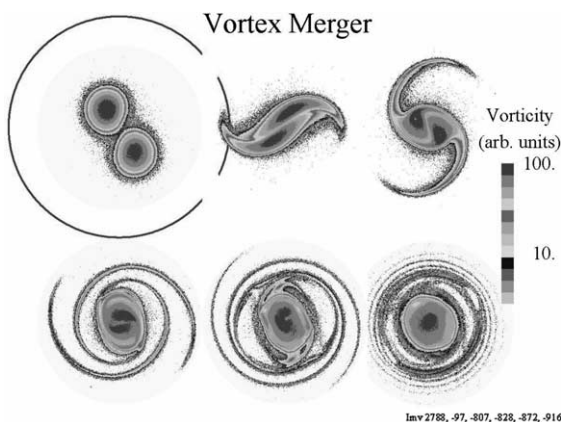


Fig. 3. Merger of two vortices in $1/2\tau_R$.

However, the $10^4:1$ ratio attests to the weakness of “viscous” effects, and suggests an effective Reynolds number $Re \approx 10^4-10^5$.

Some of the circulation originally trapped in the two individual vortices is “lost” to filamentation; these filaments eventually get stretched and mixed to finer spatial scales than can be imaged, so they form a weak “background” of vorticity. This background then influences the dynamics of the intense vortices.

4. Vortex/background dynamics

The dynamics of intense positive vortices (clumps) or negative vortices (holes) on a non-uniform background of vorticity has been extensively analyzed [18,19]. The analysis clearly shows that clumps move *up* the background vorticity gradient, and holes move *down* the gradient. Fig. 4 shows this effect in a numerical simulation.

This interaction of clumps and holes with a background vorticity gradient plays an important role in 2D hydrodynamics. For example, the motion of hurricanes on a rotating planet is influenced by the north–south gradient in the Coriolis parameter, which can be thought of as a (potential) vorticity gradient [18].

These clumps and holes must be classified as prograde or retrograde, depending on whether they rotate with or against the local background shear [19]. A straightforward linear analysis of the flow perturbation generated by the vortex correctly gives the motion of a retrograde vortex. In contrast, prograde vortices are always non-linear and move at a slower rate; and this slower rate is given by a simple “mix-and-move” estimate.

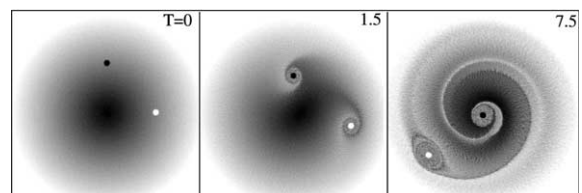


Fig. 4. Gradient-driven radial motion of a clump and hole in a circular shear flow.

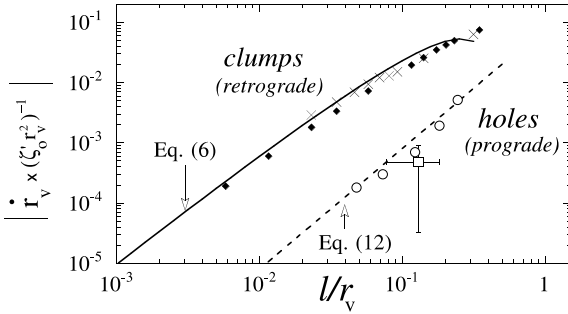


Fig. 5. Radial velocity of clumps and holes from theory, simulation, and experiments.

Fig. 5 shows the (scaled) vortex velocity $\dot{r}_v \equiv (dr_v/dt)$ in terms of the vortex intensity as represented by its trapping length $l \equiv (\Gamma_v/2\pi S)^{1/2}$. Here, Γ_v is the vortex circulation, and $S \equiv 2\pi r \times (\partial f_R/\partial r)$ is the shear in the background flow.

5. Relaxation of turbulence

Fig. 6 shows the relaxation of fully developed turbulence. Highly filamented initial conditions rapidly form many individual vortices, which then freely relax toward a 2D meta-equilibrium [20]. In this inviscid relaxation, chaotic mutual advection and vortex merger are clearly important dynamical processes. The final “generic” meta-equilibrium is

typically strongly peaked on center, reflecting the single intense vortex resulting from repeated mergers, superimposed on a weaker background vorticity.

Surprisingly, this relaxation is sometimes halted when individual vortices settle into a stable, rotating “vortex crystal” pattern which persists for thousands of rotation times τ_R . The observed vortex crystal states consist of $N_v = 5-20$ individual vortices each 4–6 times the background vorticity, arranged in a lattice pattern which rotates with the background flow. Since the surviving vortices all have about the same circulation, the patterns are quite regular, as seen at $600\tau_R$ in Fig. 6.

In each sequence, the unstable filamentary initial condition forms $N_v = 50-100$ vortices of roughly equal circulation, after which N_v initially decreases as $N_v \sim t^{-\xi}$. This relaxation is generally consistent with a dynamical punctuated scaling theory (PST) based on conserved quantities in repeated vortex merger [21]. The observed ξ range from 0.2 to 1.1 as the initial conditions are varied, with 0.8 being commonly observed.

The measured integral quantities for both sequences are consistent with 2D inviscid motion on large scales and dissipation on fine scales. Experimentally, the circulation, angular momentum, and energy are robust invariants. In contrast, the enstrophy Z_2 is a “fragile” invariant, and initially decays a factor of about 2 in both sequences.

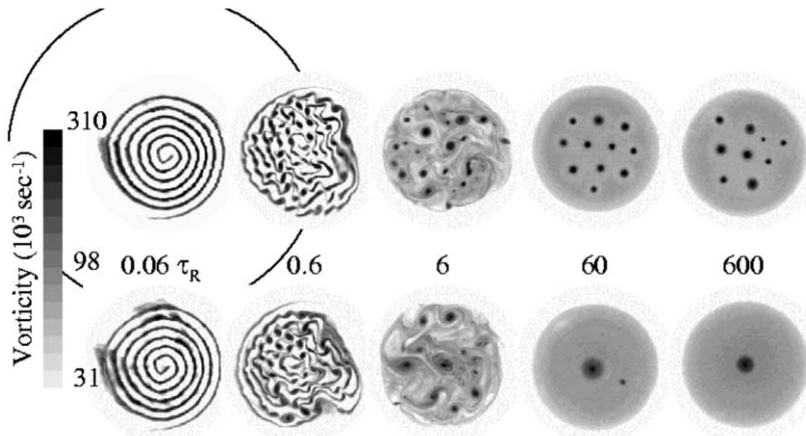


Fig. 6. Inviscid relaxations to “vortex crystals” and to a single vortex.

“Cooling” of the chaotic advective motions of the individual vortices is required to form the vortex crystal states. These random velocities decrease by a factor of 6 between $2\tau_R$ and $100\tau_R$ for the crystals sequence, whereas only slight cooling is seen before relaxation to $N_v = 1$ for the monotonic sequence.

This cooling and cessation of relaxation through mergers is a near-inviscid 2D fluid effect, i.e. it conserves energy H and is independent of the details of the fine-scale dissipation. It has now been observed in 2D simulations [22]. Only after $10^4\tau_R$ does N_v decrease to 1 as the individual vortices decay away in place due to non-ideal “viscous” effects.

However, the non-zero total circulation is essential: because there is no “negative” vorticity, the diffuse background necessarily persists, and the vortex/background interactions are more pronounced. Cooling apparently occurs through the chaotic mixing of background vorticity by the strong vortices, as opposed to processes such as deformations of individual vortices in the crystal pattern.

6. Dynamics and entropy

In recent years, two radically different theories have had some success in describing the free relaxation of 2D turbulence. One is the PST referred to above [21], which postulates that the turbulent flow is dominated by strong vortices which generally follow Hamiltonian dynamics of macroscopic point-like vortices, punctuated by the occasional merger of like-sign vortices. The relaxed state is then one single extended vortex of each sign, or just one vortex in our case as opposed to vortex crystals.

A diametrically opposite approach is incorporated in the global maximum fluid entropy (GMFE) theory [23]. This approximates the turbulent flow as a collection of non-overlapping, incompressible microscopic vorticity elements that become ergodically mixed in the relaxed state. Clearly, the GMFE theory cannot explain the vortex crystals, since the theory predicts a smooth vorticity distribution.

A new regional maximum fluid entropy (RMFE) theory approach [24,25] characterizes the vortex crystal states by maximizing the fluid entropy S [23] of the background. The key idea is that some regions of the flow are well mixed, while other regions are not. This statistical theory treats the flow only after the mergers of the strong vortices have ceased. The strong vortices then ergodically mix the background, driving it into a state of maximum fluid entropy. This mixing, in return, affects the punctuated dynamics of the strong vortices, “cooling” their chaotic motion, and driving them into an equilibrium pattern.

The diffuse background vorticity is assumed to consist of incompressible microscopic vorticity elements of fixed strength ζ_f . Coarse-graining over these randomized vorticity elements then gives the observed background vorticity $\zeta_b(r)$.

Given these inputs, two properties of the relaxed vortex crystal state can be predicted: the coarse-grained vorticity distribution of the background $\zeta_b(r)$, and the equilibrium positions $\{\mathbf{R}_i\}$ of the strong vortices [24]. The resulting background distributions are of the form

$$\zeta_b(r) = \zeta_f / (e^{\beta\zeta_f\Psi} + 1), \quad (1)$$

where $\Psi \equiv \psi + \frac{1}{2}\Omega r^2 + \mu$ is the stream function in the rotating frame, and (β, Ω, μ) are parameters. This “Fermi distribution” occurs because the microscopic vorticity elements are assumed to be incompressible. Surprisingly, the RMFE solutions reproduce the observed vortex crystal patterns and background distribution quite well.

Thus, the following physical picture of vortex crystal formation emerges: the strong vortices undergo chaotic mergers described by PST, but they also ergodically mix the low vorticity background. The mixing of the background, in return, cools the chaotic motion of the vortices, and drives the vortices into a vortex crystal equilibrium. The interaction between the strong vortices and the background, a process neglected in the PST, may be important in understanding the relaxation of 2D turbulence in other situations as well.

Interestingly, this approach [25] gives estimates for the number N_c of vortices which survive to form the vortex crystal state, by equating the time to merge to the time to cool. Here, the estimates

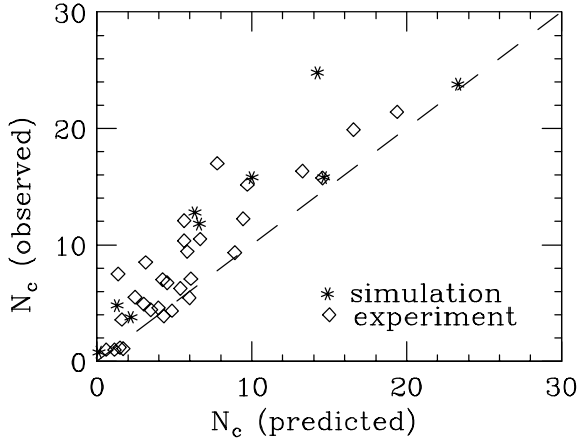


Fig. 7. Observed and predicted numbers N_c of strong vortices in the vortex crystals for simulations and experiments.

are based on the dynamical scaling exponents ζ and η , which determine the number of surviving vortices $N_v(t)$ and their total circulation $\Gamma_v(t)$ as

$$\begin{aligned} N_v(t) &= N_v(t_0) \left(\frac{t}{t_0} \right)^{-\zeta}, \\ \Gamma_v(t) &= \Gamma_v(t_0) \left(\frac{t}{t_0} \right)^{\zeta\eta}. \end{aligned} \quad (2)$$

Note that the assumptions of PST imply $\eta = 1/2$, but somewhat different values ($0.2 < \eta < 0.8$) are observed in experiments and simulations. The time to merge is given by $1/\tau_m(t) = -(d/dt)N_v$, and the cooling time is estimated from mixing arguments as $\tau_c(t) = A/\alpha N_v \Gamma_v$, where A is the area of the vorticity patch, and $\alpha \approx 0.03$. Surprisingly, these simple estimates predict N_c to within about a factor of 2, as shown in Fig. 7.

7. Point-vortex diffusion and viscosity

The microscopic discreteness of the point vortices (individual electrons) leads to “collisions” between point vortices, giving macroscopic effects such as diffusion and viscosity. These transport coefficients are now known to depend on the *shear* in the overall flow generated by the point vortices themselves.

The self-diffusion of a two-dimensional gas of interacting point vortices is a classic problem in non-equilibrium statistical physics, with relevance

to the behavior of type-II superconductors, dislocations in solids, rotating superfluid helium, and turbulence and transport in Euler fluids and plasmas. Early work on this problem focused on the case of a quiescent, homogeneous shear-free gas [26,27]. In this shear-free limit, the diffusion coefficient has the following simple form:

$$D^{\text{TM}} = \frac{1}{8\pi} \sqrt{N\gamma^2/\pi}, \quad (3)$$

where N is the number of point vortices, each with circulation γ . The diffusion coefficient is not an intensive quantity because the diffusion process is dominated by large “Taylor vortices” (regions with higher or lower density n of point vortices) whose size is of order the system size.

In electron plasmas, each electron has 2D circulation $\gamma = 4\pi ce/BL$. A dimensionless measure of the shear is

$$s(r) = \frac{2\pi r(\partial f_R/\partial r)}{n\gamma}, \quad (4)$$

i.e. the shear rate scaled by the rotation frequency of a plasma of density n in the absence of shear.

For moderate to strong shear, i.e. $|s| \gtrsim 1$, the diffusion from multiple distant collisions can be obtained [28] from a quasilinear calculation based on the Kubo formula, giving

$$D^K = \frac{\gamma}{2|s|} \ln \left(\frac{r}{d} \right). \quad (5)$$

Here, d is the minimum distance for which the vortex–vortex interaction is well described by vortices streaming past one another in the shear flow (unperturbed orbits).

Molecular-dynamics and vortex-in-cell simulations agree with this theory, provided that the shear s is *negative*. Fig. 8 shows the shear-free diffusion coefficient near D^{TM} , reduced in agreement with Eq. (5) for $s = -1.2$ and -12 . Surprisingly, however, when the shear s is *positive* the diffusion observed in the simulations is roughly an order of magnitude smaller than this theory predicts. Here, the analysis of vortex “collisions” must apparently include vortices in trapped orbits around each other.

Thus, the microscopic collisional transport theory is essentially similar to the macroscopic dy-

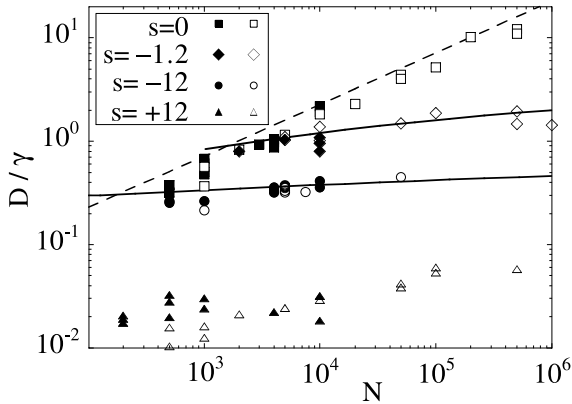


Fig. 8. Self-diffusion coefficient vs. particle number N , for shear rates $s = 0, -1.2, -12$ and 12 . Points are from simulations, lines are D^{TM} and D^{K} (dashed) from theory.

namics of 2D vortices on a background gradient, and the effects of flow shear are similar on both. Macroscopically, clumps (or holes) move up (or down) a background vorticity gradient at a rate which depends critically on whether the vortices are prograde or retrograde with respect to the overall flow shear. This distinction is new to fluid theory, but is crucial to the dynamics: a simple linear analysis predicts the motion of a retrograde vortex, but inherently non-linear trapping effects must be included to predict the (much slower) motion of a prograde vortex.

Microscopically, theory and simulations show that retrograde point vortices diffuse more rapidly than prograde vortices. A rigorous kinetic analysis predicts the diffusion of retrograde vortices, quantifying the effects of the shear in the flow; but no kinetic analysis is yet available for the diffusion of retrograde point vortices, due to the dominance of non-linear trapped orbits.

Acknowledgements

This work was supported by National Science Foundation grant PHY98-76999 and Office of Naval Research grant N00014-96-1-0239.

References

- [1] C.F. Driscoll, K.S. Fine, *Phys. Fluids* 2 (1990) 1359.
- [2] A.J. Peurrung, J. Fajans, *Phys. Fluids B* 5 (1993) 4295.
- [3] D.H.E. Dubin, *Phys. Plasmas* 5 (1998) 1688.
- [4] K.S. Fine, C.F. Driscoll, J.H. Malmberg, T.B. Mitchell, *Phys. Rev. Lett.* 67 (1991) 588.
- [5] W. Kelvin, *Nature* 23 (1880) 45.
- [6] R.J. Briggs et al., *Phys. Fluids* 13 (1970) 421.
- [7] N.S. Pillai, R.W. Gould, *Phys. Rev. Lett.* 73 (1994) 2849.
- [8] A.C. Cass, Ph.D. dissertation, UCSD, 1998.
- [9] D.A. Schecter et al., *Phys. Fluids* 12 (2000) 2397.
- [10] M.T. Montgomery, C. Lu, *J. Atmos. Sci.* 54 (1997) 1868.
- [11] T.B. Mitchell, C.F. Driscoll, *Phys. Rev. Lett.* 73 (1994) 2196.
- [12] R.H. Levy, *Phys. Fluids* 8 (1965) 1288.
- [13] R.C. Davidson, *Physics of Nonneutral Plasmas*, Addison-Wesley, New York, 1990.
- [14] C.F. Driscoll et al., in: *Plasma Physics and Controlled Nuclear Fusion Research*, vol. 3, IAEA, Vienna, 1989, p. 507.
- [15] C.F. Driscoll, *Phys. Rev. Lett.* 64 (1990) 645.
- [16] R.A. Smith, M.N. Rosenbluth, *Rev. Lett.* 64 (1990) 649; R.A. Smith, *Phys. Fluids B* 4 (1992) 287.
- [17] T.J. Hilsabeck, T.M. O'Neil, *Phys. Plasmas* 8 (2001) 407.
- [18] G.F. Carnevale et al., *J. Fluid Mech.* 233 (1991) 119.
- [19] D.A. Schecter, D.H.E. Dubin, *Vortex Motion Driven by a Background Vorticity Gradient*, 1999.
- [20] K.S. Fine, A.C. Cass, W.G. Flynn, C.F. Driscoll, *Phys. Rev. Lett.* 75 (1995) 3277.
- [21] G.F. Carnevale et al., *Phys. Rev. Lett.* 66 (1991) 2735; J.B. Weiss, J.C. McWilliams, *Phys. Fluids A* 5 (1993) 608.
- [22] D.A. Schecter, D.H.E. Dubin, K.S. Fine, C.F. Driscoll, *Phys. Fluids* 11 (1999) 905.
- [23] J. Miller, *Phys. Rev. Lett.* 65 (1990) 2137; R. Robert, J. Sommeria, *J. Fluid Mech.* 229 (1991) 291; J. Miller, J.B. Weichman, M.C. Cross, *Phys. Rev. A* 45 (1992) 2328, and references therein.
- [24] D.Z. Jin, D.H.E. Dubin, *Phys. Rev. Lett.* 80 (1998) 4434–4437.
- [25] D.Z. Jin, D.H.E. Dubin, *Phys. Rev. Lett.* 84 (2000) 1443.
- [26] J.B. Taylor, B. McNamara, *Phys. Fluids* 14 (1971) 1492.
- [27] J.M. Dawson, H. Okuda, R.N. Carlile, *Phys. Rev. Lett.* 27 (1971) 491.
- [28] D.H.E. Dubin, D.Z. Jin, *Phys. Lett. A* 284 (2001) 112.